

# Split off-specular reflection and surface scattering from woven materials

Sylvia C. Pont and Jan J. Koenderink

We measured radiance distributions for black lining cloth and copper gauze using the convenient technique of wrapping the materials around a circular cylinder, irradiating it with a parallel light source and collecting the scattered radiance by a digital camera. One family of parallel threads (weave or weft) was parallel to the cylinder generator. The most salient features for such glossy plane weaves are a splitting up of the reflection peak due to the wavy variations in local slopes of the threads around the cylinders and a surface scattering lobe due to the threads that run along the cylinder. These scattering characteristics are quite different from the (off-)specular peaks and lobes that were found before for random rough specular surfaces. The split off-specular reflection is due to the regular structures in our samples of man-made materials. We derived simple approximations for these reflectance characteristics using geometrical optics. © 2003 Optical Society of America

*OCIS codes:* 080.0080, 160.0160, 240.0240.

## 1. Introduction

Reflections from rippled surfaces have been described in some inspiring literature, such as Minnaert's<sup>1</sup> book on light and color in the outdoors and Montagu Pollock's<sup>2</sup> book on light and water. These authors discuss the shape, size, and color of reflections from rippled water surfaces, such as pillar-like reflections from the sun on the sea, and other viewpoint-specific phenomena, such as light coils on gently undulating water. Angle-dependent functions for the statistics of the sun's glitter on the sea surface in terms of the statistics of the slope distribution are useful for estimations of the roughness of the sea surface.<sup>3,4</sup> However, most authors did not consider the distribution of the reflectance as a function of the viewing and lighting angles. Derivations for the bidirectional reflectance distribution function (for a definition see Ref. 5) have been studied for random rough locally specular surfaces. Studies in the realm of physical and geometrical optics (see, for instance, Refs. 6–10) assume surface geometries that can be represented by statistical distributions of micro-facet orientations. Such models predict specular peaks, off-specular peaks,

and specular lobes due to reflections from (statistical distributions of) surface undulations. They do quite well in describing many kinds of natural materials.

The aim of this paper is to study angle-dependent reflections from man-made materials that consist of highly regular wave-like structures at scales of human vision. A common example of such structures are weaves of specularly reflecting threads, for example, shiny fabrics like silk and lining cloth or gauze, with surface undulation dimensions that (can be resolved visually and thus) are much larger than the wavelength of the incident light (for instance, daylight). Such materials call for deterministic descriptions instead of statistical ones and for an approach from the realm of geometrical (ray) optics instead of physical (wave) optics. Lu<sup>11</sup> studied the optical properties of shot fabrics, which have warps and fillings that are dyed different colors. She showed that the viewing direction dependent color changes of these fabrics were due mainly to an occlusion effect.

## 2. Empirical Study

We measured the reflectance from plane weavings of shiny (primarily specularly reflecting) threads: black lining cloth, fine and coarse copper gauze, and shot fabrics composed of reddish and greenish threads. The setup is depicted schematically in Fig. 1. Notice that the different parts in Fig. 1 were scaled differentially and that measurements were taken at scales of human vision. The materials were wrapped around a 4.6-cm wide circular cylinder with one family of

The authors are with the Helmholtz, Princetonplein 5, 3584 CC Utrecht, the Netherlands.

Received 30 July 2002; revised manuscript received 30 October 2002.

0003-6935/03/081526-08\$15.00/0

© 2003 Optical Society of America

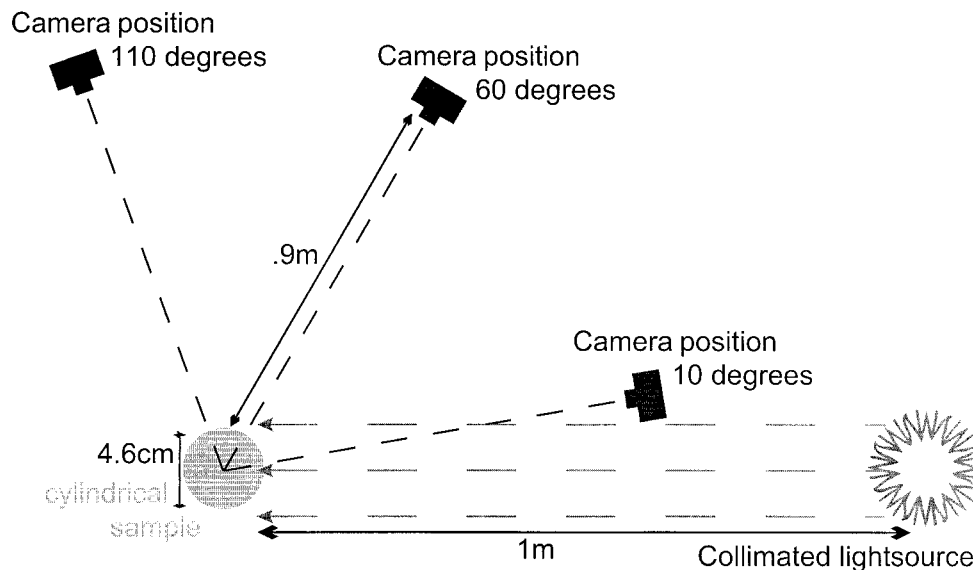


Fig. 1. Schematic depiction of the experimental setup; the different components of the setup were scaled differently in this figure. The cylindrical sample with a diameter of 4.6 cm was positioned upright, at the center of a frame with two arms that could be rotated around that center. The collimated light source was placed at one arm and the camera at the other arm, such that the phase angle could be varied. Here we show the positions of the camera that were used for the empirical study: 10°, 60° and 110°.

threads parallel to the generator of the cylinder and illuminated with a parallel light source (a Xenon arc source with a small aperture). This method, which was introduced by Lu *et al.*,<sup>12</sup> allows to take measurements for a large range of illumination and viewing angles in one shot. The scattered radiance was collected with a Leaf Lumina digital scan CCD camera with a linear response and an effective dynamic range of 12 bits, which was positioned at a distance of .9 m from the sample on a frame that could be rotated around the sample. Measurements were done in a darkroom with black painted walls. We chose three phase angles between the light source and the camera that span a large range: 10°, 60°, and 110°.

In Fig. 2 we show the photographs of the cylindrical 4.6-cm wide samples and the corresponding pixel values for horizontal cross-sections of the images. The pixel values represent the radiance, because the camera has a linear response. Pixel values are represented as a function of the azimuthal angle around the cylinder. For all three samples we find a specular lobe that is bounded by a split (off-)specular peak. For the copper gauze we find that the lobe is broader for the gauze that is coarser. At grazing illumination and viewing angles surface scattering occurs, which can be seen at both the left- and right-hand sides of the cylinders covered with copper gauze for a phase angle of 10° and only at the left-hand sides at all other photos. In the images of the coarse copper gauze it can be traced visually where the separate specularities come from; the modulations in the graphs are due to the surface geometry and not to noise. The dimensions of these undulations are of the order of tenths of millimeters to millimeters, which is much larger than the wavelength of the incident light, justifying a geometrical optics approach. The photo-

graphs suggest that the main characteristics of the reflectances, the split off-specular peak and the surface scattering, might be due to reflections from the threads around the cylinder and those parallel to the cylinder axis, respectively.

Because the reflections from the threads around the cylinder and those from the threads along the cylinder seem to have different effects on the radiance distributions, we also did a measurement for shot fabrics (see Ref. 11). In Fig. 3 we show two measurements of a sample of shot fabrics composed from reddish wefts and greenish warps (wrapped around a 4.6-cm wide cylinder), which were done under a phase angle of 10°. The orientation of the fabrics was changed by 90° between the two measurements, and it is clear that this orientation difference results in quite spectacular color changes. Of course, a red and green visual appearance does not mean that isolated threads would show up as pure red and pure green in RGB levels (the reflectance spectra usually cover a broad spectrum, and the RGB channels of the camera filter over quite broad wavelength ranges as well). The graphs directly underneath the photographs show the pixel values of the separate R, G, and B channels combined in one plot, and in the next row the G/R ratio for the horizontal cross-sections (averaged over the columns in the images). It is clear that if the color of the doubled reflection peak in the middle is reddish, the surface scattering at grazing angles has a greenish color, and vice versa for the other orientation of the cloth. The splitting up of the specular peak is clear in one case, but in the other case it can hardly be detected.

### 3. Theory

In this section we derive formal descriptions of the two main characteristics of the reflectance of specular

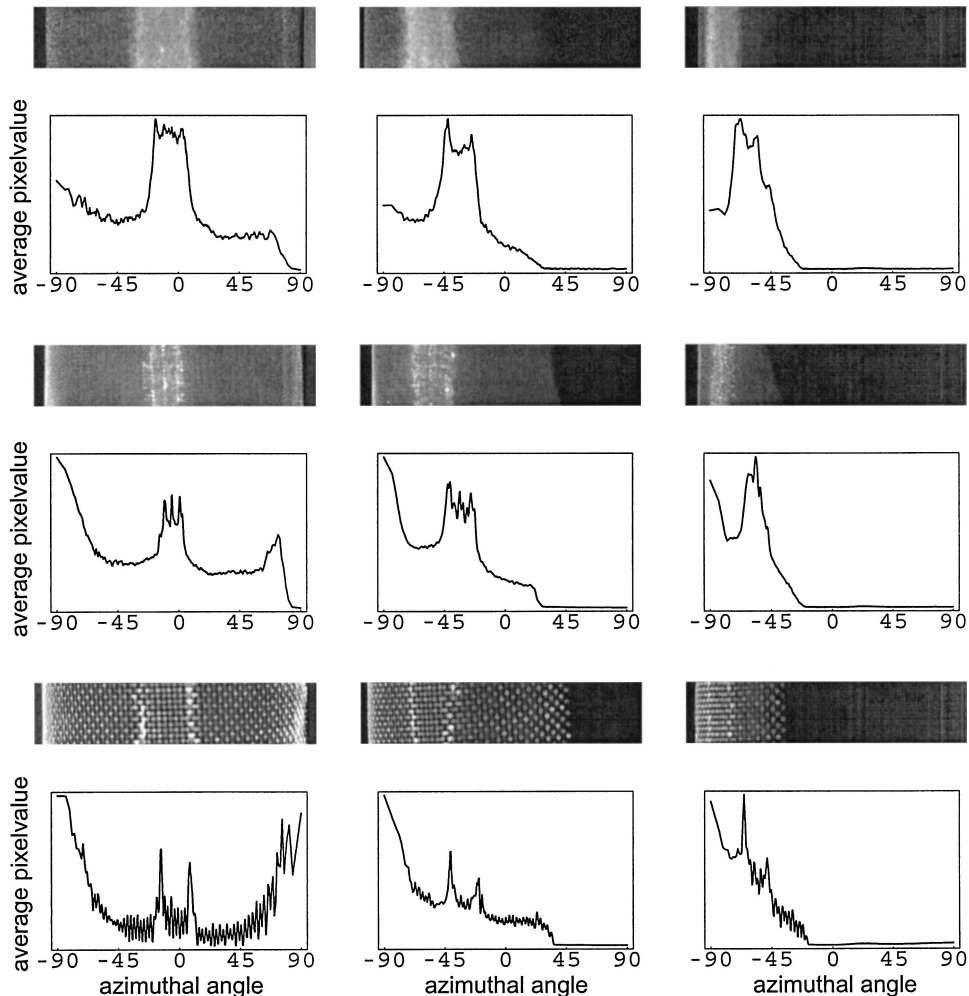


Fig. 2. Photographs of 4.6 cm wide cylinders covered with silk (upper row), fine copper gauze (middle row) and coarse copper gauze (lower row), which are all plane weaves. The pictures were taken for phase angles between the collimated light source and the camera of 10°, 60°, and 110°. With these photographs we show the pixelvalues that were averaged over columns parallel to the cylinder axis. These values reflect radiance, because the camera has a linear response. It is clear that the specular lobe is bounded by a split (off-)specular peak. The peak is broader if the gauze is coarser. Another characteristic of the reflectance is the surface scattering at grazing illumination and viewing angles, which can be seen at both the left-hand and right-hand sides of the cylinders for a phase angle of 10° and only at the left-hand sides for the other phase angles. The fine structure in the graphs for the coarse copper is due to the geometrical structure of the gauze (the effect of individual wires being visible), not to noise.

weavings or gauzes. We consider materials for which the dimensions of the surface undulations are much larger than the wavelength of the incident light, and therefore, we use geometrical (ray) optics, not physical (wave) optics. First, we present a simple two-dimensional description of reflections from a sine wave, for which the main reflectance phenomenon is a doubling of the specular peak. Second, we consider the surface-scattering phenomenon for tangential threads.

Consider a sine-wave-shaped thread illuminated by a parallel light source (see Fig. 4). We use a Cartesian coordinate system  $\{x, y\}$ . Let the direction of the incident beam be denoted as  $\mathbf{i}$ , and the direction of the exit beam  $\mathbf{j}$  (with  $\mathbf{i} \cdot \mathbf{i} = \mathbf{j} \cdot \mathbf{j} = 1$ ). We only consider the plane of incidence (that is, in this case, the X–Y plane). If the local normal on the cylinder is denoted as  $\mathbf{n}$ , then  $\mathbf{j} = 2(\mathbf{n} \cdot \mathbf{i})\mathbf{n} - \mathbf{i}$ . The

incident direction is determined by an angle  $\theta$  with respect to the fiducial normal (the plane's global normal) such that  $\mathbf{i} = (\sin \theta, \cos \theta)$ . Rays from an angle  $\theta$  are reflected from the thread in the direction  $\mathbf{j}$  that is determined by the angle  $\psi$  with respect to the fiducial normal. The angles  $\psi$  and  $\theta$  are both measured clockwise with respect to the fiducial normal). A pencil of parallel entrance rays will be reflected to an output pencil with a certain angular spread, which depends on the local curvature of the thread. The radiance from the thread is proportional with

$$I = \frac{E_0(\mathbf{i} \cdot \mathbf{n})}{\left| \frac{\partial \psi}{\partial x} \right|}. \quad (1)$$

We assume that the shape of the threads can be approximated by a sinusoidal function

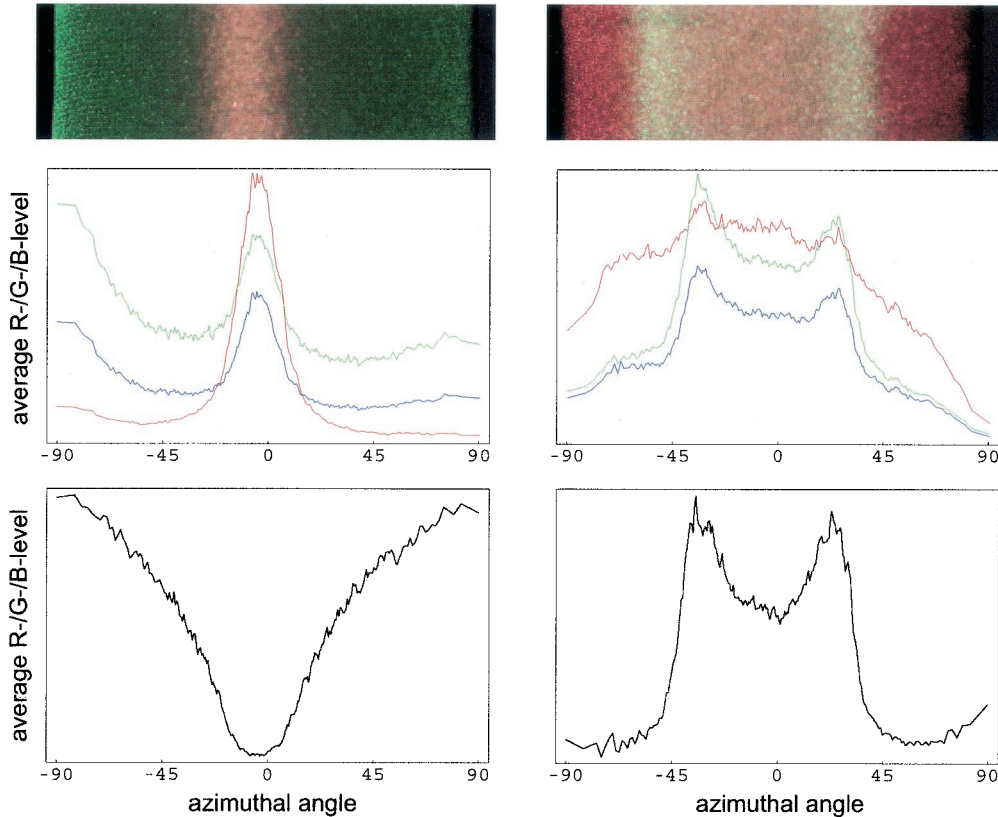


Fig. 3. Cangiate silk (or “shot silk”) composed from reddish and greenish threads (note that a red and green appearance doesn’t mean that isolated threads would show up as pure red and pure green in RGB-levels). The photographs were both taken of the same piece of silk, which was wrapped around a 4.6-cm diameter cylinder, the only difference being that the orientation of the cloth differs by 90°. The phase angle was 10°. Instead of the gray levels of the pixels (as in Fig. 2) we now depict the separate R, G, and B levels, in the first row of the graphs. In the lower row we show the ratio between the G and R levels. For one orientation we find that the color of the doubled reflection peak in the middle is reddish, while the surface scattering at grazing angles has a greenish color (left-hand side column). For the other orientation of the cloth we find reversed colors (right-hand side column). The splitting up of the specular peak is clear in one case (the right-hand side one), but in the other case (the left-hand side one) it can hardly be detected. This difference is due to geometrical differences of warp and weft threads.

$h(x) = h_0 \sin kx$  with an amplitude  $h_0$  and wavelength  $\lambda = 2\pi/k$  (so  $h'(x) = kh_0 \cos kx$  and  $h''(x) = -k^2 h_0 \sin kx$ ), see Fig. 5, top left-hand side. The local outward normal on the thread surface is then  $\mathbf{n} = (-h'(x), 1)/[1 + h'(x)^2]^{1/2}$ . The exit angle is  $\psi = -\theta - 2 \arctan h'(x)$ , see Fig. 5, middle left. Then we find that

$$\left| \frac{\partial \psi}{\partial x} \right| = \frac{|2h''(x)|}{1 + [h'(x)]^2} \quad (2)$$

see Fig. 5, lower left-hand side. Together this results in

$$I = \frac{E_0 \{1 + [h'(x)]^2\}^{1/2} [-h'(x) \sin \theta + \cos \theta]}{|2h''(x)|} \quad (3)$$

To find an expression as a function of viewing and illumination angles (in the far field), we can substitute  $x = (1/k) \arccos [(1/kh_0) \tan (-(\psi + \theta)/2)]$ , which

was derived from the equations for  $\psi$  and  $h'(x)$ . Finally this all results in

$$I = \frac{E_0 \left| \cos \left( \frac{\psi - \theta}{2} \right) \right|}{2k \cos^2 \left( \frac{\psi + \theta}{2} \right) \left[ h_0^2 k^2 - \tan^2 \left( \frac{\psi + \theta}{2} \right) \right]^{1/2}}, \quad (4)$$

which is depicted in Fig. 5 at the right-hand side for  $k = 1$ ,  $h_0 = 0.2$ , and three angles of incidence of 0°, 30°, and 60°, as a function of the azimuthal angle around a cylinder (as in the graphs of the empirical data). The main characteristic of the reflectance is a lobe that is bounded at both angular extrema by reflectance peaks. The width of the lobe or, in other words, the angular distance between the split off-specular reflection peaks is determined by  $\psi + \theta = \pm 2 \arctan kh_0$  and in this manner related to the surface geometrical structure. Thus, if the illumination angle  $\theta$  is constant, the distance between the viewing angles for which we will find reflection peaks is 4

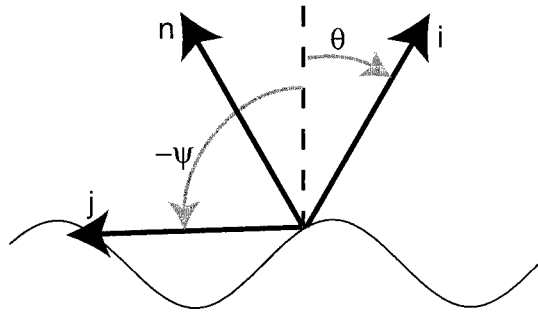


Fig. 4. Schematic representation of the geometry. We assume that the woven silk and copper gauze can be represented by a composition of sinusoidal threads. Here, we consider a single thread. If a ray hits the thread from a direction  $\mathbf{i}$  (under an angle  $\theta$  with respect to the global surface normal) at a position with local surface normal  $\mathbf{n}$ , it will be reflected in the direction  $\mathbf{j}$  (under an angle  $\psi$  with respect to the global normal).

$\arctan kh_0$ . For the cylindrical samples the viewing and illumination angles covary ( $\psi = \theta + \alpha$  with  $\alpha$  the phase angle) and thus the angular difference between the reflection peaks is equal to  $2 \arctan kh_0$ . Figure 6 may promote an intuitive grasp of this theory. The

height at the specular point ( $\psi = -\theta$ ) is  $(E_0 \cos \theta) / (2k^2 h_0)$ . In the next section we will use the first measure to do some semi-quantitative estimates of the structure of the silk and copper gauze samples that were used in our empirical study (see Fig. 1).

The former paragraph concerned the split off-specular reflection peak that we found for plane specular weavings. Next, we derive an approximation for the second feature of their reflectances, the surface-scattering characteristic. Consider a circular cylinder illuminated by a parallel light source and covered with locally curved threads that run along the cylinder generator (see Fig. 7). Beckmann and Spizzichino<sup>6</sup> showed that a surface element  $dS$  with principal radii of curvature  $r_1$  and  $r_2$  will scatter the incident energy into a solid angle

$$d\Omega = \frac{4dS \cos \theta}{r_1 r_2}. \quad (5)$$

Then, with  $I = (E_0 dS \cos \theta) / d\Omega$  and  $r_1 r_2 = Rd/2$  with  $d$  the thickness of the thread, we find that  $I = E_0 r_1 r_2 / 4 = E_0 Rd / 8$ . Finally, we take into account that the density of visible threads increases toward the edges of the cylinder:  $N(y) = N_0 / \cos \theta_v$ , with  $N_0$  the num-

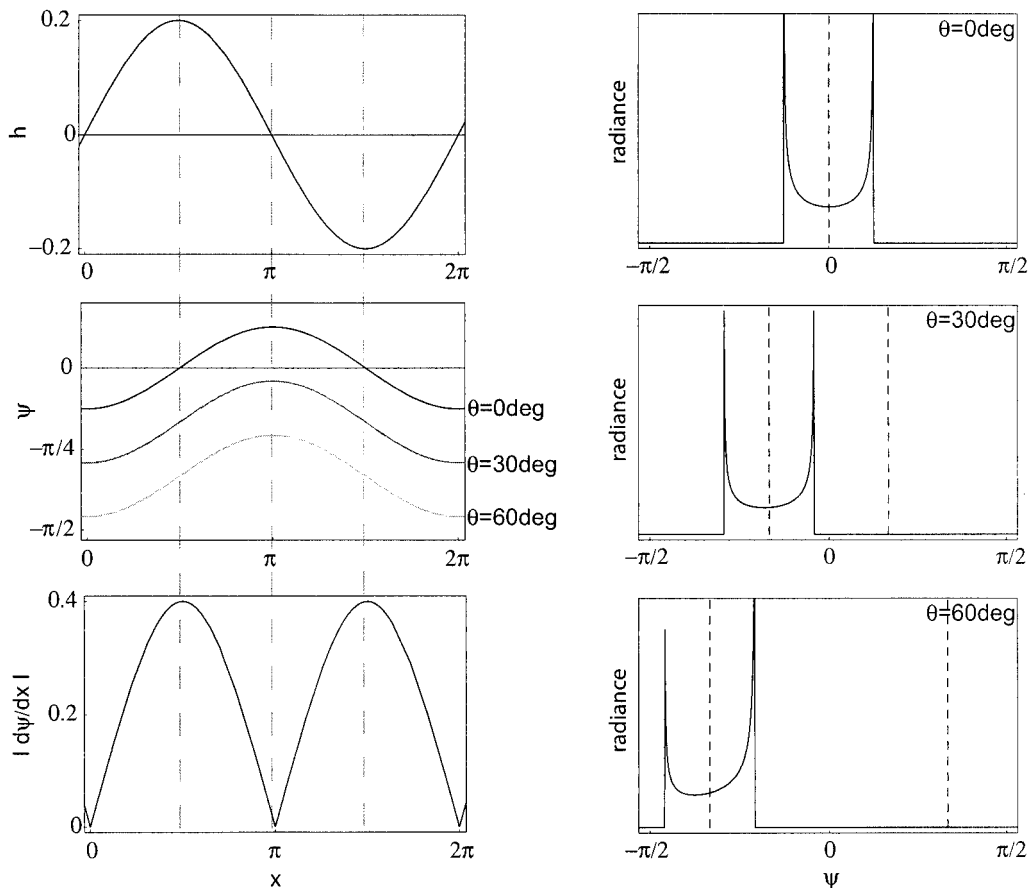


Fig. 5. Graphs of a sine wave with amplitude 0.2 and wavelength  $2\pi$  (top left-hand side), the exit angle  $\psi$  as a function of the position of reflection on the sine wave for three different angles of illumination (middle left-hand side) and the derivative of the former graph (lower left-hand side). At the right we show the resulting radiance as a function of viewing angle for illumination angles  $0^\circ$  (top right-hand side),  $30^\circ$  (middle right-hand side) and  $60^\circ$  (lower right-hand side).

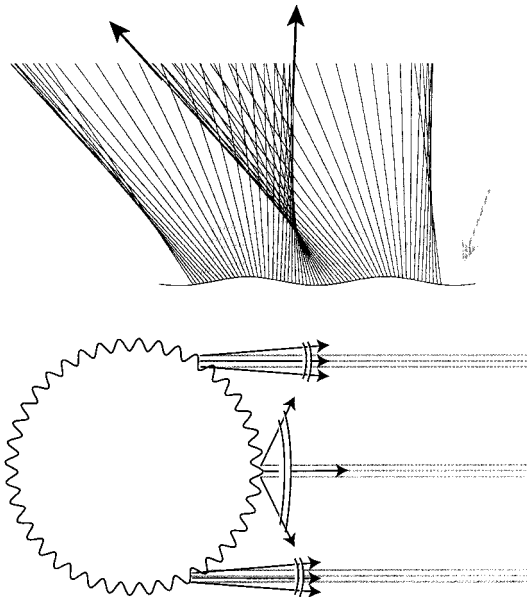


Fig. 6. This figure depicts the mechanism behind the splitting up of the specular reflection peak for a wave-like structure on a plane (top figure) or a wave-like structure that is wrapped around a cylinder (top view in lower figure). In the top figure light rays hit the surface from the direction depicted by the gray arrow (and separate rays by the gray lines) and scatter in several directions (black lines). The reflected radiance has a bimodal structure in the far field with maxima represented by the black arrows. Consider light rays from a collimated beam that illuminate the cylinder head-on (gray lines), and assume the viewing direction is also head-on. (It is easy to extrapolate the ideas to other geometrical lay outs.) The rays that will hit the cylinder at the position at which the global normal is perpendicular to the illumination direction ( $P_s$ ) will scatter over quite a large angle due to the large variation of the local normal. There are two areas for which the spread of the scattered rays is very small (far-field caustics) at both sides of  $P_s$ : the two specular peaks. At these locations the rays reflect at the inflection points of the sinusoid which represent almost planar (zero curvature) facets.

ber of longitudinal threads visible for normal viewing and  $y$  the axis across the cylinder. (Here, we ignore the possible interference of the effects of occlusion.) The final result,  $I = N_0 E_0 R d / 8 \cos \theta_s$ , is shown in Fig. 8. It is a clear example of a surface-scattering lobe, similar to what is found in black velvet, for instance (see Refs. 12 and 13).

#### 4. Semi-Quantitative Analysis

The simplest semi-quantitative analysis for the cylindrical samples is an estimation of the peak-to-peak width, which should equal  $2 \arctan kh_0$ . This estimate can be done without further (photometrical) calibration, in contradiction to the estimates of the geometry of the surface from the height  $(E_0 \cos \theta) / (2k^2 h_0)$ , for which we need  $E_0$ . For the coarse copper gauze sample we estimated the peak-to-peak width from the photograph profiles:  $22^\circ$ . This value was compared with one that was calculated on the basis of measurements of the thread thicknesses and distances between threads using a microscope. We as-

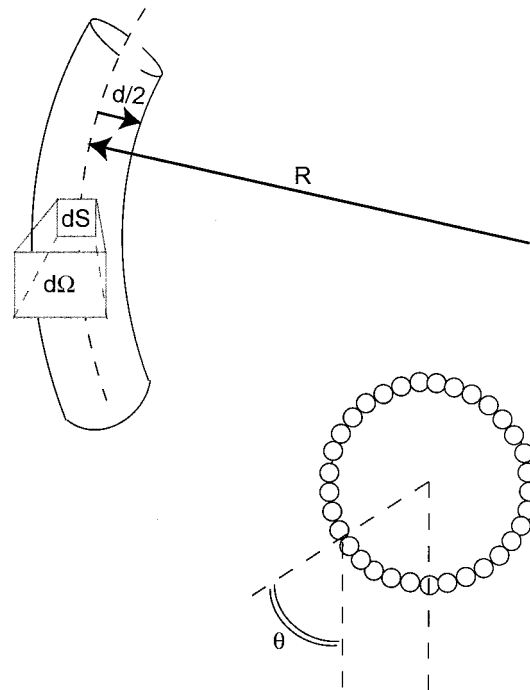


Fig. 7. Depiction of the geometrical layout for the longitudinal threads. Rays reflect on a surface element  $dS$  with principal radii of curvature that are determined by the curvature of the thread  $R$  and the thickness of the thread  $d$  into a solid angle  $d\Omega$ .

sumed that the thread thickness equals the amplitude  $h_0$ . Our microscopical study resulted in estimates of the undulation wavelength  $2\pi/k$  of 2.88 mm and of the undulation amplitude  $h_0$  of 0.108 mm, which results in an estimate of the maximum local attitude of  $\arctan kh_0 = \arctan[(2\pi/2.88 \text{ mm}) \cdot 0.108 \text{ mm}] = 13.5^\circ$  and thus an estimate of the peak-to-peak distance of  $27^\circ$ . This estimate is in the right ballpark. It is probable that the difference is caused by deviations of the surface geometry from the assumed sinusoidal shape. Closer study of a separate copper thread revealed that the geometry tends to a regular symmetric sawtooth. In that case the maximum local attitude would be approximately  $\arctan(0.216 \text{ mm}/1.44 \text{ mm}) = 8.5^\circ$ , and the peak-to-peak

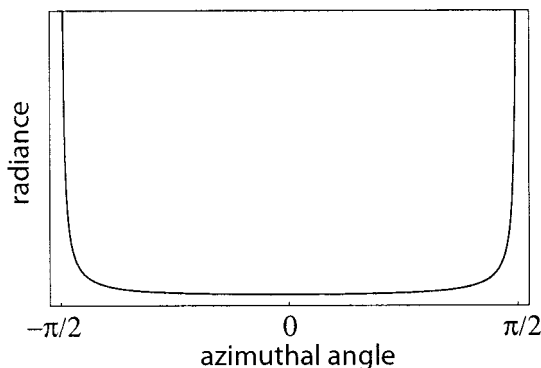


Fig. 8. Scattered luminance as a function of the azimuthal angle around the cylinder for threads along the cylinder.

estimate for the cylindrical sample  $17^\circ$ . Other effects that can cause differences are vignetting and reflexes, especially for waves with relatively large amplitudes.

## 5. Conclusions

Mesoscale plane weaves of specularly reflecting threads show split (off-)specular peaks and surface scattering. We studied these characteristics using samples that were wrapped around 4.6 cm cylinders, such that all features of the reflectance distribution were visible in all separate measurements. The characteristics could be modeled in simple ways by use of geometrical optics. A two-dimensional model of specular reflection from a sine wave explains the split off-specular peaks, which are the boundaries of a specular lobe. Another model of scattering from locally curved threads, taking into account that the density of the visible threads changes as a function of the viewing angle, predicts surface scattering. Surface scattering was found before and described in a more general framework as asperity scattering.<sup>13</sup> Lu *et al.*'s<sup>11</sup> study on shot fabrics did describe color effects due to occlusion effects. The surface scattering and split reflection peak weren't clearly identifiable in her data, which is probably due to the fact that they only measured colored shot fabrics. For copper gauze or black lining cloth the reflectance is almost completely determined by the specular reflection, and therefore the peaks must be more pronounced than in the case when there is a relatively large diffuse component.

Specular peaks, off-specular peaks, and specular lobes were described before,<sup>6-10</sup> but not split specular peaks. Viewpoint-dependent phenomena such as the distribution of specular points on rippled-water surfaces were also discussed.<sup>1,2,4,14</sup> The link between these near- and far-field descriptions can be seen in Fig. 6; the far-field description yields two peaks in the reflectance distribution at the asymptotes of the caustic.

Our samples are quite common materials. Although they are of course man-made, there are lots of examples of such woven (or waved, in a deterministic sense) surfaces in our daily surroundings; all sorts of shiny woven fabrics, such as silk and lining cloth, rippled plastics, or, for instance, corrugated iron. Similar natural surfaces are rippled carapaces of some varieties of beetles (for instance the Domino beetle; a carabid beetle of the Genus *Anthea*) or leaves that include a regularly rippled pattern in their structure. In Fig. 9 we show three examples. The first example is a draped net curtain which is composed of red (roughly running horizontally in this layout) and blue (running vertically) threads. Folds that are approximately vertical cause red split off-specular reflections and horizontal folds cause blue split reflections. The second example is an eggcup for which we find a quite broad reflection lobe, which is due to relatively large deviations of the local attitudes in comparison with the fiducial normal at the surface. The third photograph of a tea-strainer

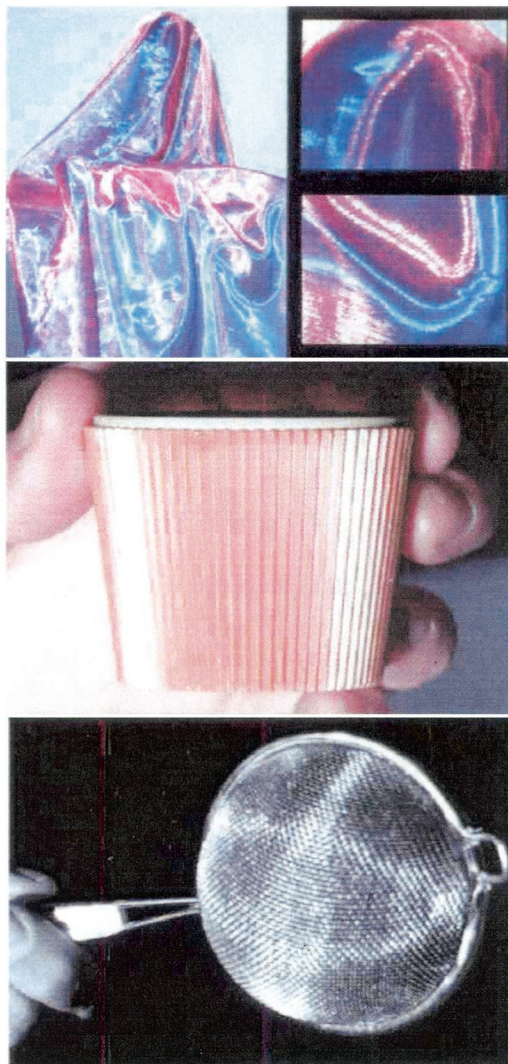


Fig. 9. Examples of split off-specular peaks in three common objects. The first photograph shows a draped glossy net curtain, which is composed from red and blue threads. Two details in which the split off-specular peaks are clearly visible are shown enlarged at the right. The specular reflections are red or blue, depending on the shape of the cloth and the direction of the threads. For this layout, approximately, red specular peaks are found at vertical folds and blue at horizontal folds. (And indeed the red threads run horizontally and the blue vertically.) The second example is an eggcup with a rippled surface, for which the split specular reflection peaks are found to be quite far apart. (And indeed the maximum local attitudes at the surface were quite large.) The last example is a tea strainer, for which we find two perpendicular split reflection stripes. (And indeed the convex shaped gauze is basically composed of perpendicularly woven threads.)

shows two perpendicular split specular reflection stripes, which are due to the perpendicularly woven metal threads and the strainer's convex shape. The brighter areas at the lower and left-hand side of the strainer are due to surface scattering. The optical properties of these materials, doubled specular peaks and surface scattering, do not fit in the conventional general reflectance frameworks which combine a sin-

gle (off-)specular peak with a specular lobe and a diffuse lobe.<sup>15</sup> We were able to describe the mechanisms underlying these reflectance characteristics of woven and rippled surfaces with simple geometrical optics.

## References and Note

1. M. G. J. Minnaert, *Light and Color in the Outdoors* (Springer-Verlag, New York, 1993).
2. B. Montagu Pollock, *Light and water. A Study of Reflexion and Colour in River, Lake and Sea* (George Bell and Sons, London, 1903).
3. M. S. Longuet-Higgins, "The statistical analysis of a random, moving surface," *Philos. Trans. R. Soc. London* **249**, 321–387 (1957).
4. C. Cox and W. Munk, "Measurement of the roughness of the sea surface from photographs of the sun's glitter," *J. Opt. Soc. Am.* **44**, 838–850 (1954).
5. F. E. Nicodemus, J. C. Richmond, and J. J. Hsia, *Geometrical Considerations and Nomenclature for Reflectance* (Natl. Bur. Stand. (U.S.) Monogr. 160 (1977).
6. P. Beckman and A. Spizzichino, *The Scattering of Electromagnetic Waves from Rough Surfaces* (Pergamon Press, New York, 1963).
7. B. van Ginneken, M. Stavridi, and J. J. Koenderink, "Diffuse and specular reflection from rough surfaces," *Appl. Opt.* **37**, 130–139 (1998).
8. S. K. Nayar, "Surface reflection: physical and geometrical perspectives," *IEEE Transactions on Pattern Anal. Mach. Intell.* **13**, 611–634 (1991).
9. M. Oren and S. K. Nayar, "Generalization of the Lambertian model and implications for machine vision," *Int. J. Comput. Vision* **14**, 227–251 (1995).
10. K. E. Torrance, E. M. Sparrow, and R. C. Birkebak, "Polarization, directional distribution, and off-specular peak phenomena in light reflected from roughened surfaces," *J. Opt. Soc. Am. A* **56**, 916–925 (1966).
11. R. Lu, J. J. Koenderink, and A. M. L. Kappers, "Optical properties (bidirectional reflectance distribution function) of shot fabric," *Appl. Opt.* **39**, 5785–5795 (2000).
12. R. Lu, J. J. Koenderink, and A. M. L. Kappers, "Optical properties (bidirectional reflectance distribution function) of velvet," *Appl. Opt.* **37**, 5974–5984 (1998).
13. J. J. Koenderink and S. C. Pont, "The secret of velvety skin," *Mach. Vision Appl. special issue on Human Modeling, Analysis and Synthesis*.
14. J. J. Koenderink, "Trieste in the mirror," *Perception* **29**, 127–133 (2000).
15. J. D. Foley, A. van Dam, S. K. Feiner, and J. F. Hughes, *Computer Graphics, Principles and Practice* (Addison-Wesley, Reading, Mass., 1990).